

JUNGBIN PARK¹, JUNHYUB JEON¹, NAMHYUK SEO¹, GWANGHUN KIM¹,
SEUNG BAE SON¹, JAE-GIL JUNG¹, SEOK-JAE LEE^{1*}

AUSTENITIC STABILITY AND STRAIN-INDUCED MARTENSITIC TRANSFORMATION BEHAVIOR OF NANOCRYSTALLINE FeNiCrMoC HSLA STEELS

The austenitic stability and strain-induced martensitic transformation behavior of a nanocrystalline FeNiCrMoC alloy were investigated. The alloy was fabricated by high-energy ball milling and spark plasma sintering. The phase fraction and grain size were measured using X-ray diffraction. The grain sizes of the milled powder and the sintered alloy were confirmed to be on the order of several nanometers. The variation in the austenite fraction according to compressive deformation was measured, and the austenite stability and strain-induced martensitic transformation behavior were calculated. The hardness was measured to evaluate the mechanical properties according to compression deformation, which confirmed that the hardness increased to 64.03 HRC when compressed up to 30%.

Keywords: nanocrystalline; austenite stability; strain-induced martensite; transformation-induced-plasticity

1. Introduction

Recently, many studies have been conducted to improve the fuel efficiency of various means of transportation in response to carbon emission regulations. Medium-carbon low-alloy steel containing Ni, Cr, and Mo is a representative high-strength low-alloy (HSLA) steel widely used in mechanical parts such as aircraft landing gears, automobile structural parts, gears, and shafts [1-5]. Therefore, in order to improve fuel efficiency, it is essential to reduce the weight of these parts. However, good mechanical properties are also required because these components are repeatedly subjected to high stress. Therefore, research on HSLA steel with good mechanical properties relative to their weight is essential.

Powder metallurgy is a well-known method for obtaining good mechanical properties without increasing the amount of alloying elements added [6]. It has been reported that nanocrystalline alloy powder can be manufactured by repeated cold welding and fracture of the powder through high-energy ball milling [7,8]. The spark plasma sintering (SPS) method can sinter the powder within a short sintering time, so it is suitable for suppressing the growth of crystallites [9,10]. Nanosized crystallites improve

the mechanical properties of materials by the Hall-Petch effect [11,12]. Many studies have been reported on sintered alloys with nanosized crystallites and good mechanical properties through high-energy ball milling and SPS [13-16].

The increased fraction of retained austenite is another advantage of ultrafine-grain steel manufactured by powder metallurgy. Recently, several studies have reported that a much higher fraction of retained austenite is observed owing to the ultrafine particle effect [17-19]. This is because the nanosized crystallites of the sintered alloy produced by powder metallurgy are much finer than those of a wrought alloy. Retained austenite is known to improve the toughness and tensile strength of steels by the transformation-induced plasticity (TRIP) effect, in which the retained austenite transforms into strain-induced martensite during plastic deformation [20-23]. Therefore, to improve the mechanical properties of HSLA steel used for structural parts, research on austenite stability is required, but it is still insufficient. To solve this deficiency, in this study, an ultrafine HSLA sintered alloy was prepared using powder metallurgy, and the austenite stability and martensitic transformation behavior of the sintered alloy were investigated.

¹ JEONBUK NATIONAL UNIVERSITY, RESEARCH CENTER FOR ADVANCED MATERIALS DEVELOPMENT, DIVISION OF ADVANCED MATERIALS ENGINEERING, JEONJU 54896, REPUBLIC OF KOREA

* Corresponding author: seokjaelee@jbnu.ac.kr



2. Experimental

The initial powder consisted of Fe (99% purity, average particle size <math><75\ \mu\text{m}</math>, Höganäs), Ni (99% purity, average particle size 3-7 $\mu\text{m}</math>, Alfa Aesar), Cr (99% purity, average particle size 149 $\mu\text{m}</math>, Alfa Aesar), Mo (99.95% purity, average particle size 3-7 $\mu\text{m}</math>, Alfa Aesar), Mn (99.6% purity, average particle size 10 $\mu\text{m}</math> or less, Alfa Aesar), Si (99.99% purity, average particle size 44 $\mu\text{m}</math> or less, Alfa Aesar), and graphite (purity 99%, average particle diameter 7-11 $\mu\text{m}</math>, Alfa Aesar). The alloy composition was Fe-0.41C-1.72Ni-0.76Cr-0.21Mo-0.77Mn-0.29Si (wt.%), which is similar to that of AISI 4340 steel classified as a representative HSLA steel. As a process control agent, stearic acid [$\text{CH}_3(\text{CH}_2)_{16}\text{CO}_2\text{H}</math>, Alfa Aesar] was added at 1% by weight. Mechanical alloying of the powder was performed for 24 h at 250 rpm in an Ar atmosphere using high-energy ball-milling equipment (FRITSCH, Pulverisette-6). The ball milling was stopped for 30 min after milling for 1 h. The ball-to-powder (BPR) ratio was set to 30:1, and stainless-steel balls were used for milling. After the mechanical alloying was completed, the powder was placed in a graphite mold with an inner diameter of 10 mm and sintered using SPS. For sintering, the graphite mold was heated to 1000°C at a rate of 1000°C/min in a vacuum atmosphere to which a uniaxial pressure of 70 MPa was applied. The sample was then cooled in the chamber. The microstructure and phase analysis of the sintered alloy were analyzed using X-ray diffraction (XRD, Shimadzu, XRD-6100). To evaluate the mechanical properties and TRIP behavior, hardness tests (SSAUL BESTECH, BSETROC-300N) and compression tests (general purpose tester, Instron 5569) were performed.$$$$$$$

3. Results and discussion

Fig. 1 shows the XRD patterns of the milled FeNiCrMoC powders. Only the ferrite alpha peak was detected in the pattern of the milled powder, indicating that mechanical alloying was complete. The crystallite size of the milled powder was calculated using the Williams-Hall equation for the XRD patterns [24].

$$\beta_r \cos \theta = \frac{\kappa \cdot \lambda}{D} + \eta \sin \theta \quad (1)$$

where β is the full width at half maximum (FWHM) of the XRD peaks, θ is the Bragg angle, k is a constant, λ is the wavelength of the Cu K α target (=1.5406 Å), D is the crystallite size, and η is the strain. The crystallite size of the milled powder was calculated to be approximately 7.4 nm. During high-energy ball milling, cold welding and fracturing occur repeatedly to produce nanosized crystallite powders [7,8].

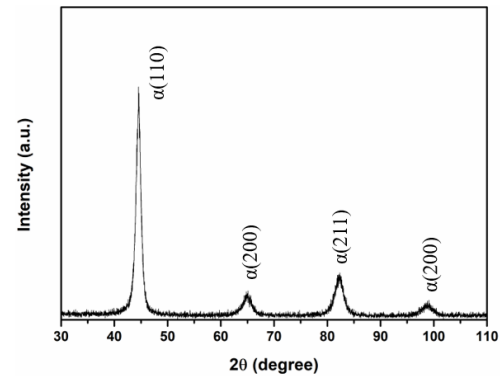


Fig. 1. XRD patterns of the FeNiCrMoC milled powder

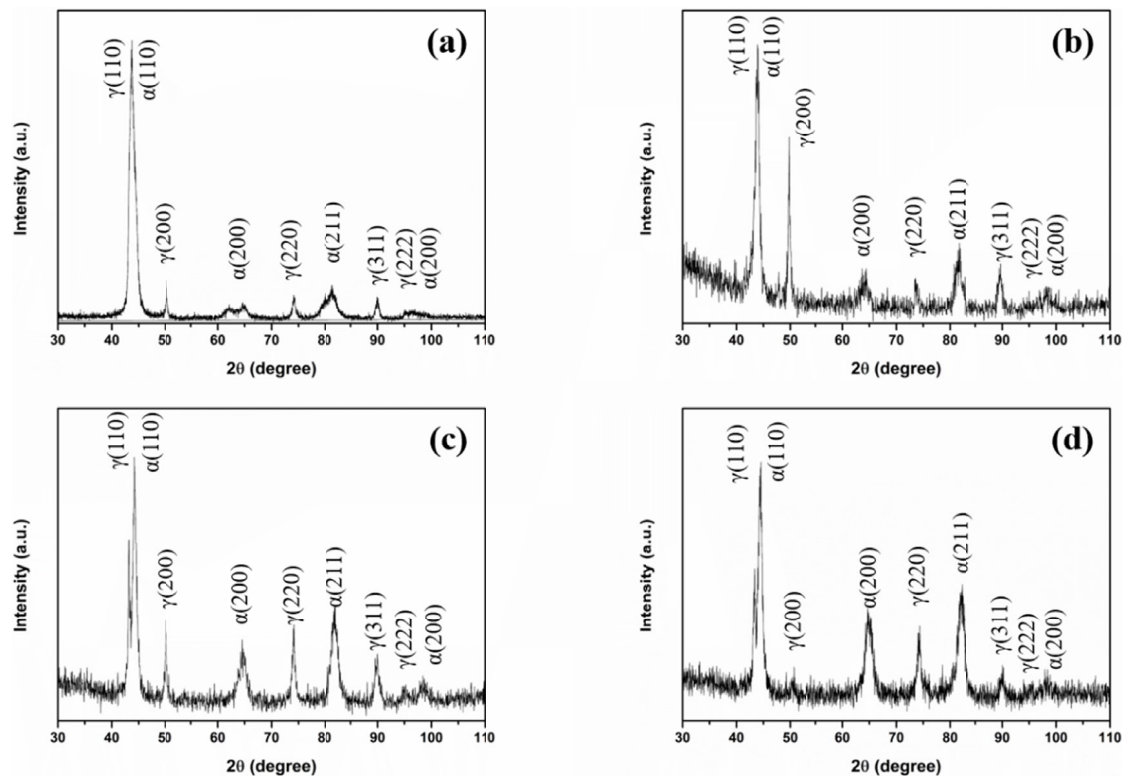


Fig. 2. XRD patterns of (a) as-sintered and (b) 10% deformed, (c) 20% deformed, and (d) 30% deformed specimens

Fig. 2 shows the XRD patterns of the as-sintered specimen and the specimen subjected to a compressive deformation of 10-30%. Ferrite alpha and austenite beta peaks are observed in the as-sintered and deformed specimens, and it can be seen that the austenite peak strength changes as the amount of deformation increases. The crystallite size of the sintered alloy was calculated to be approximately 7.7 nm because the growth of crystallites is inhibited by rapid sintering through SPS [9,10].

Fig. 3 and Table 1 show the decrease in the volume fraction of austenite and the change in hardness according to each condition calculated using the XRD pattern in Fig. 1. The austenite volume fraction was calculated using the Averbach-Cohen model based on the XRD pattern results [25].

$$V_{\gamma} = \frac{\frac{I_{\gamma(200)} + I_{\gamma(220)} + I_{\gamma(311)}}{3}}{\frac{I_{\alpha(200)} + I_{\alpha(220)}}{2} + \frac{I_{\gamma(200)} + I_{\gamma(220)} + I_{\gamma(311)}}{3}} \quad (2)$$

where V_{γ} is the austenite volume fraction, and I_{γ} and I_{α} are the intensities of the austenite and ferrite peaks, respectively. The austenite fraction of the as-sintered specimen was measured to be 50.61 vol.%, which is significantly higher than that of conventional HSLA steel [26,27]. This is because the austenite stability was increased by the fine nanosized crystallites, as calculated above [16-18]. As the compressive strain increased from 10% to 30%, the austenite volume fraction decreased. The hardness of the as-sintered specimen was 60.47 HRC, which is 2.4 times higher than that of commercial HSLA steel with a similar composition (approximately 25-48 HRC) [28-33]. This is because the crystallite size was much finer than that of conventional commercial HSLA steel, and the hardness was improved by the Hall-Petch effect. The hardness increased to 64.03 HRC at 30% strain. Thus, it was confirmed that TRIP occurs when plastic deformation is applied, transforming the soft retained austenite into hard martensite.

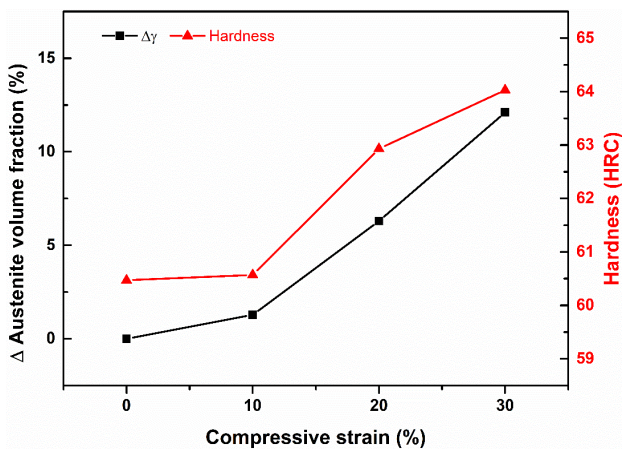


Fig. 3. Relationship between the volume fraction of austenite and the change in hardness according to the compressive strain

We adopted the Burke-Matsumura-Tsuchida (BMT) model to quantitatively express the strain-induced martensitic trans-

TABLE 1

Change in austenite volume fraction and hardness

Compressive strain	Austenite vol. frac. (%)	Hardness (HRC)
as-sintered	50.61 ± 2.15	60.47 ± 0.29
10%	49.33 ± 2.33	61.02 ± 0.29
20%	44.31 ± 1.98	62.93 ± 0.21
30%	38.05 ± 2.77	64.03 ± 0.45

formation rate as a function of plastic deformation [34-36]. The equation of the BMT model is

$$V_{\alpha'} = V_{\gamma}^0 / \left(1 + \frac{p}{k \varepsilon^p V_{\gamma}^0} \right) \quad (3)$$

where $V_{\alpha'}$ is the volume fraction of strain-induced martensite, V_{γ}^0 is the initial volume fraction of austenite, k is a constant related to austenite stability, ε is the plastic strain, and p is the autocatalytic strain exponent. It has been reported that although the p value is 1 when the autocatalytic effect is 0, the martensitic transformation kinetics can be accelerated by reducing the austenite grain size [18,37,38]. The crystallite size of the sintered alloy produced in this study was several nanometers, so the p value was set to 2. The higher the austenite stability, the lower the k value. The average k value, according to the amount of deformation in this study was 14.03. Fig. 4 shows a comparison of the strain-induced martensite transformation behavior predicted using Eq. (3) and the volume fraction measured according to the compressive strain.

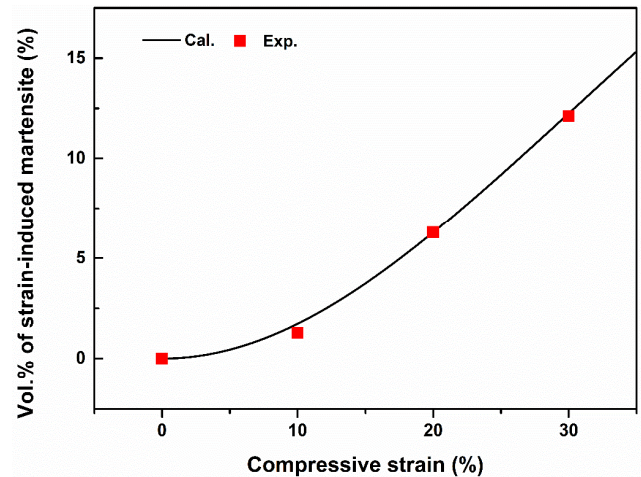


Fig. 4. Comparison of strain-induced martensite behavior calculated by BMT model and actual measured fraction

The change in the fraction of strain-induced martensite calculated using the equation was found to have a coefficient of determination (R^2) of 0.985. In addition, it can be seen that the proposed formula and the strain-induced martensite transformation behavior analysis using it are very reliable because the proposed formula and the actual value are almost identical when compared with the measured fraction.

4. Conclusions

In this study, the austenite stability and strain-induced martensitic transformation behavior of FeNiCrMoC HSLA steel prepared by high-energy ball milling and SPS were investigated. The crystallite sizes of the milled powder and the sintered alloy were calculated to be approximately 7.4 and 7.7 nm, respectively. The sintered body showed a high retained austenite volume fraction of up to 50.61%, and it was confirmed through XRD that austenite was transformed into strain-induced martensite when compressively deformed from 10% to 30%. The hardness was 60.47 HRC at 0% strain, and it increased to 64.03 HRC at 30% strain. The austenite stability was calculated using the BMT model. In addition, the strain-induced martensite transformation rate for the amount of plastic deformation was calculated using the BMT model, and the transformation behavior was evaluated by comparing it with the actual measured fraction.

Acknowledgments

This work was supported by a Korea Institute for Advancement of Technology grant, funded by the Korea Government (MOTIE) (P0002019), as part of the Competency Development Program for Industry Specialist. This work was supported by the Technology Innovation Program (20011879) funded by the Ministry of Trade, Industry & Energy (MOTIE, Korea).

REFERENCES

- [1] R. Karimbaev, Y.S. Pyun, E. Maleki, O. Unal, A. Amanov, *Mater. Sci. Eng. A* **791**, 139752 (2020).
- [2] W.S. Lee, T.T. Su, *J. Mater. Process. Technol.* **87**, 198 (1999).
- [3] Y. Tomita, *Metall. Trans. A* **22A**, 1093 (1991).
- [4] G.Y. Lai, W.E. Wood, R.A. Clark, V.F. Zackay, E.R. Parker, *Metall. Mater. Trans. B* **5**, 1663 (1974).
- [5] R.L. McDaniels, S.A. White, K. Liaw, L. Chen, M.H. McCay, P.K. Liaw, *Metall. Trans. A* **485**, 500 (2008).
- [6] J.S. Benjamin, T.E. Volin, *Met. Trans.* **5** 1929 (1974).
- [7] H.J. Fecht, E. Hellstern, Z. Fu, W.L. Johnson, *Metall. Trans. A* **21**, 2333 (1990).
- [8] C. Keller, K. Tabalaiev, G. Marnier, J. Noudem, X. Sauvage, E. Hug, *Mater. Sci. Eng. A* **665**, 125 (2016).
- [9] V. Mamedov, *Powder Metall.* **45**, 322 (2002).
- [10] Z. Shen, M. Johnsson, Z. Zhao, M. Nygren, *J. Am. Ceram. Soc.* **85**, 1921 (2002).
- [11] E.O. Hall, *Proc. Phys. Soc. B* **64**, 747 (1951).
- [12] N.J. Petch, *J. Iron Steel Inst. Jpn.* **174**, 25 (1953).
- [13] G. Kim, J. Jeon, N. Seo, S. Choi, M.S. Oh, S.B. Son, S.J. Lee, *Arch. Metall. Mater.* **66**, 759 (2021).
- [14] J. Jeon, S. Choi, N. Seo, Y.H. Moon, I.J. Shon, S.J. Lee, *Arch. Metall. Mater.* **65**, 1249 (2020).
- [15] S.G. Choi, J.H. Jeon, N. Seo, Y.H. Moon, I.J. Shon, S.J. Lee, *Arch. Metall. Mater.* **65**, 1001 (2020).
- [16] M.J. Chae, A. Sharma, M.C. Oh, B. Ahn, *Met. Mater. Int.* **27**, 629 (2021).
- [17] N. Seo, J. Jeon, G. Kim, J. Park, S.B. Son, S.J. Lee, *J. Korean Powder Metall. Inst.* **27**, 373 (2020).
- [18] G. Kim, J. Jeon, N. Seo, J. Park, S.B. Son, S.J. Lee, *J. Korean Powder Metall. Inst.* **28**, 246 (2021).
- [19] S.J. Oh, D. Park, K. Kim, I.J. Shon, S.J. Lee, *Mater. Sci. Eng. A* **725**, 382 (2018).
- [20] M.R. Berrahmoune, S. Berveiller, K. Inal, A. Moulin, E. Patoor, *Mater. Sci. Eng. A* **378**, 304 (2004).
- [21] S. Lee, B.C. De Cooman, *Metall. Mater. Trans. A* **44A**, 5018 (2013).
- [22] B.C. De Cooman, *Curr. Opin. Solid State Mater. Sci.* **8**, 285 (2004).
- [23] N. Saeidi, M. Jafari, J.G. Kim, F. Ashrafzadeh, H.S. Kim, *Met. Mater. Int.* **26**, 168 (2020).
- [24] G.K. Williamson, W.H. Hall, *Acta Metall.* **1**, 22 (1953).
- [25] B.L. Averbach, M. Cohen, *Trans. AIME* **176**, 401 (1948).
- [26] C.N. Sastry, K.H. Khan, W.E. Wood, *Metall. Trans. A* **13A**, 676 (1982).
- [27] R.O. Ritchie, R.M. Horn, *Metall. Trans. A* **9A**, 331(1978).
- [28] M.M. Bilal, K. Yaqoob, M.H. Zahid, U.H. Ehsan, W.H. Tanveer, A. Wadood, B. Ahmed, *J. Mater. Res. Technol.* **8**, 5194 (2019).
- [29] S. Zhirafar, A. Rezaeian, M. Pugh, *J. Mater. Process. Technol.* **186**, 298 (2007).
- [30] P. Phetlam, V. Uthaisangsuk, *Mater. Des.* **82**, 189 (2015).
- [31] N. Niazi, S. Nisar, A. Shah, *Int. J. Mater. Sci. Eng.* **5**, 6 (2014).
- [32] M. Houssny-Emam, M.N. Bassim, *Mater. Sci. Eng.* **61**, 79 (1983).
- [33] I. Polyzois, N. Bassim, *Mater. Sci. Eng. A* **631**, 18 (2015).
- [34] J. Burke, *Kinetics of Phase Transformation in Metals*, Pergamon Press, Oxford, United Kingdom, 1965.
- [35] O. Matsumura, Y. Sakuma, H. Takechi, *Scr. Mater.* **21**, 1301 (1987).
- [36] N. Tsuchida, Y. Tomota, *Mater. Sci. Eng. A.* **285**, 345 (2000).
- [37] S.J. Oh, B.C. Kim, M.C. Suh, I.J. Shon, S.J. Lee, *Arch. Metall. Mater.* **64**, 863 (2019).
- [38] D. Park, S.J. OH, I.J. Shon, S.J. Lee, *Arch. Metall. Mater.* **63**, 1479 (2018).